



Interfacial Properties of β -Lactoglobulin at the Oil/Water Interface: Influence of Starch Conversion Products with Varying Dextrose Equivalents

Theresia Heiden-Hecht¹ · Marco Ulbrich² · Stephan Drusch¹ · Monika Brückner-Gühmann¹

Received: 11 June 2020 / Accepted: 11 November 2020
© The Author(s) 2020

Abstract

In spray dried emulsions, frequently milk proteins are used as interfacial active components and starch conversion products are added as matrix material at high concentrations. To characterize interfacial properties at the oil/water interface by commonly applied methods, low protein, and carbohydrate concentrations from 1 to 2% are usually analyzed. The impact of a higher concentration of starch conversion products was not investigated so far. Therefore, the formation and rheological properties of β -lactoglobulin (β -LG) stabilized films at the oil/water interface were investigated via short and long-time adsorption behavior using pendant drop tensiometry as well as dilatational and interfacial shear rheology. Suitability of the applied methods to the chosen samples with higher concentrations >1–2% was verified by calculation of selected key numbers like capillary number and by detailed reviewing of the results which is summarized further on as key indicators. It is hypothesized, that the increase in concentration via presence of starch conversion products will delay interfacial stabilization as a result of increased bulk viscosity with decreasing degree of degradation (dextrose equivalent) of the starch. Furthermore, this increase in concentration leads to more stable interfacial films due to thermodynamic incompatibility effects between protein and starch conversion products which results in increases of local protein concentration. Key indicators proved a general suitability of applied methods for the evaluation of the investigated samples. Moreover, results showed an increase in interfacial film stability and elastic properties alongside a decreased interfacial tension if starch conversion products were present in a high concentration.

Keywords Dilatational rheology · Interfacial shear rheology · β -Lactoglobulin · Starch conversion product · Excluded volume effect · Application related concentration

✉ Theresia Heiden-Hecht
t.heiden-hecht@tu-berlin.de

Marco Ulbrich
marco.ulbrich@tu-berlin.de

Stephan Drusch
stephan.drusch@tu-berlin.de

Monika Brückner-Gühmann
monika.brueckner-guehmann@tu-berlin.de

¹ Technische Universität Berlin, Faculty III Process Sciences, Institute of Food Technology and Food Chemistry, Department of Food Technology and Food Material Science, Straße des 17. Juni 135, 10623 Berlin, Germany

² Department of food process engineering, Technische Universität Berlin, Seestraße 13, 13353 Berlin, Germany

Introduction

Oil in water emulsions are dispersed food systems that may be used in many different contexts. In emulsions high molecular weight emulsifiers like proteins may be present. Proteins lower the interfacial tension and stabilize the o/w interface. [1]. The process of interfacial stabilization by proteins can be divided into four stages: (1) protein migration through the bulk, (2) protein adsorption at the interface, (3) conformational reorganization of the protein and (4) formation of a stable interfacial film with intermolecular cross-linkings [2–4]. Owing to its ability to provide stability to food emulsions β -LG is one of the most thoroughly investigated high molecular weight emulsifiers. Its interfacial properties were found to depend on several external factors like environmental conditions e.g. pH, temperature and ionic strength [5–11].

In order to convert β -LG stabilized emulsions into powder, spray drying is a process commonly applied in the food industry. Starch conversion products are added to increase the dry matter content of the emulsions to 45% and above and to ensure the encapsulation of the oil drops in the emulsions. If proteins and polysaccharides are present in an aqueous system, different thermodynamic phenomena may occur, either co-solubility or incompatibility resulting in complexation or phase separation [12]. Co-solubility is represented by coexisting molecules while the incompatibility occurs as phase segregation of the two molecules and the complexation of proteins and polysaccharides is reflected in an associative behavior between both of them [12]. These thermodynamic mechanisms within the bulk phase will affect the resulting interfacial properties. As a result from the incompatibility between protein and polysaccharide, Rodriguez Patino and Pilosof (2011) assumed a film with a higher protein load at the interface [13]. This incompatibility, resulting from the excluded volume effect, was also verified by Antipova and Semenova (1997) using a light scattering method [14].

Since Antipova and Semenova (1997), Baeza et al. (2004); Baeza et al. (2005) and Perez et al. (2010) observed that the interfacial tension was dependent on the type of proteins and polysaccharides, it can be assumed that the molecular structure of the starch conversion products will affect the extent of the described effects [14–17]. In addition, the molecular structure of the starch conversion products commonly known as dextrose equivalent (DE) will influence the viscosity of the bulk phase [18]. This should in turn influence the diffusion based short time adsorption transport to the interface, as described in the Stokes-Einstein equation as one part of the Ward-Tordai adsorption theory [19].

Typically, adsorption kinetics and interfacial properties are investigated via drop tensiometry and interfacial shear rheology. In this context, the former can be used to characterize the adsorption to the interface at different time scales as well as the impact of expansion and compression on the characteristics of the interfacial film, while the latter describes the interactions within the interfacial film [20–22]. Both methods are typically used to characterize interfacial properties of substances under aqueous, highly diluted conditions (e.g. [10, 11, 23]). However, it can be reasonably assumed that changes in physical values like bulk viscosity, flow behavior or density will affect the interfacial properties. In addition, Bertsch and Fischer (2019 and 2020) and Bertsch et al. (2018, 2020) showed that bulk viscosity increase by gelation superimposed to interfacial stabilization can result in misinterpretation of interfacial shear rheological results [24–27]. So far, no study systematically analyzed the applicability of the interfacial methods at an increased concentration far beyond the common concentrations of 1–2%. However, the suitability of the measurement equipment as well as the model-based calculations

can be verified via specific indicators for accuracy of measurement and calculation [28–32].

Therefore, the aim of this study is to evaluate the suitability of drop tensiometry and interfacial shear rheology for the characterization of film formation and interfacial properties at an oil/water interface in systems with a dry matter content of 35% in the water phase. Moreover, the influence of different degrees of degradation in the starch conversion products should also be investigated.

It is assumed that accurate results of interfacial rheological methods can be gained at a high dry matter content in the water phase for Newtonian fluids if the effect of changes in sample characteristics in viscosity and density on interfacial measurement and derived results can be controlled. For drop tensiometry measurements an appropriate balance of interfacial tension and gravitational forces in dependence on drop volume and needle diameter needs to be maintained for accurate Young Laplace fitting. A prerequisite for dilatational rheology is the prevention of critical and droplet deforming capillary forces. For interfacial shear rheology, minimal motion of the subphase needs to be guaranteed. These prerequisites for accurate interfacial rheological methods are met by careful consideration of the following key numbers: Bond and Worthington number, capillary number and Boussinesq number.

Furthermore, it is hypothesized, that the increase in dry matter content in the water phase via addition of starch conversion products will delay interfacial stabilization as a result of increased bulk viscosity with decreasing dextrose equivalent (DE). The high dry matter content in the water phase will further lead to lower interfacial tension and more stable interfacial films with an increase in intermolecular interactions and elastic response of the viscoelastic β -LG-film due to the increase in local protein concentration caused by thermodynamic incompatibility effects between protein and starch conversion products. Therefore, pendant drop analysis with a two-fluid needle is used to characterize the adsorption behavior. The interfacial film is characterized in its viscoelasticity and strength of its intermolecular network via response of the interfacial area to expansion and compression by dilatational rheology and via nondestructive oscillation by interfacial shear rheology, respectively [20, 21].

Materials and Methods

β -LG was isolated from whey protein isolate (Bipro, Agropur Dairy Cooperative Inc., Minnesota, USA) with a method described elsewhere [33]. The resulting protein powder has a dry matter of $90.7 \pm 1.0\%$ and a protein content of $90.1 \pm 1.2\%$, while the protein content is composed of 98.11% isolated β -LG, 0.37% α -lactalbumin and 1.51% denaturated β -LG (analyzed according to Keppler et al. 2014). Medium-chain-triglyceride oil (MCT-oil) WITARIX® MCT 60/40 was

kindly provided from IOI Oleo GmbH (Hamburg, Germany). Interfacial active substances in the MCT-oil were removed via magnesium silicate adsorption (Florisil®, Carl Roth GmbH, Karlsruhe Germany). Glucose syrup with a DE of 37.3 (GS 37, C*Dry™ GL 01934), maltodextrin with a DE of 13.9 (MD 14, C*Dry™ MD 01910) and maltodextrin with a DE of 8.8 (MD 9, C*Dry™ MD 01958) were purchased from Cargill Deutschland GmbH (Krefeld, Germany). The starch conversion products differ in their dextrose equivalent that means their hydrolyzation grade of starch. The dextrose equivalent is a measure of the reducing power of the starch which is calculated as dextrose and expressed as percentage of dry matter [34]. All starch conversion products had negligible protein residues (0.1–0.15%, measured with DUMATHERM, C. Gerhardt GmbH & Co. KG, Königswinter, Germany). Distilled water was used for all experiments.

Molecular Characterization of Starch Conversion Products by Means of Size Exclusion Chromatography - Multi Angle Light Scattering - Differential Refractive Index (SEC-MALS-DRI)

Aqueous solutions of the starch conversion products were prepared by dissolving in water at a concentration 2.5 d.m.%. The solutions were diluted 1:10 (v/v) in dimethyl sulfoxide (DMSO) preheated at 40 °C to a concentration of about 2.5 mg/mL and passed through PTFE filters (Carl Roth GmbH & Co. KG, Karlsruhe, Germany) before analysis.

The molecular characterization was carried out by means of SEC-MALS-DRI as described elsewhere [35]. The separation was executed with a SEC-3010 module (WGE Dr. Bures GmbH & Co. KG, Dallgow-Doberitz, Germany) including degasser, pump and auto sampler connected to a MALS detector (Bi-MwA, Brookhaven Instruments Corporation, Holtsville, NY, USA) and a differential refractive index detector (DRI). The samples were eluted with degassed DMSO (Carl Roth GmbH & Co. KG, Karlsruhe, Germany) containing 0.1 M NaNO₃ at a flow rate of 0.5 mL/min and a temperature of 70 °C. Data were collected and processed using ParSEC Enhanced V5.61 chromatography software to give the concentration of the eluted solution at each retention volume (SEC chromatograms). This method provides no differentiation between branched and linear molecule structures since the separation is according to the hydrodynamic volume. Therefore, the results indicate mainly the molecular size of the starch conversion products.

Preparation of Protein and Protein/Starch Conversion Product-Solutions

For dilatational and interfacial shear rheological measurements protein- and protein/starch conversion product-solutions were prepared. β-LG was dissolved and stirred

in distilled water for approximately 2 h and reached a pH around 7. The starch conversion product was pre-solubilized in distilled water with usage of a stirring device (RCT Basic, IKA-Werke GmbH & Co. KG) for approximately 2 h and the pH was adjusted to 7 with 1 M NaOH. Both solutions were combined to obtain concentrations of 0.1% protein and 34.9 d.m.% starch conversion product, were stirred for further 3 h and were stored at 5 °C for about 14 h overnight. Afterwards, all solutions were stirred to obtain a homogenous solution before measurement. The pH was adjusted if necessary.

For the adsorption behavior measurement, separate protein and starch conversion product solutions were prepared in the same way as described above with a protein concentration of 1.5% and a starch conversion product concentration of 15.96%. Both solutions are combined in a particular ratio in a two-fluid needle to reach a protein concentration of 0.1% and a starch conversion product concentration of 14.9%. Here, a lower starch conversion product concentration was used due to limited file size and recording time of the video.

Characterization of Physical Values

All solutions were characterized in physical values - viscosity and density. Viscosity was determined with a flow plot from 0.1–1000 1/s under usage of a cylinder (double gap, DG 26.7), a Physica MCR 102 and MCR 501 rheometer (Anton Paar GmbH, Ostfildern, Germany). Density was determined with an oscillating U-tube (DMA 35, Chempro/Paar GmbH). The experiments were performed in triplicate.

Time Dependent Adsorption Behavior

Time dependent adsorption behavior was measured by pendant drop tensiometry (OCA-20, Dataphysics Instruments GmbH, Filderstadt, Germany) at 22 °C. A high speed camera is used to record the drop shape. The improved Young Laplace eq. (1) is fitted to the drop curvature of the drop profile while the curvature is defined with the changing tangent angle to the length at the drop curvature. With computational calculation the interfacial tension is determined.

$$\frac{d\varphi}{ds} = 2 - \frac{\Delta\rho g R_0^2 z}{\gamma} - \frac{\sin\varphi}{r} \quad (1)$$

The eq. (1) takes account of the change in tangent angle ($d\varphi$) to the change in length (ds) at the drop curvature, the cylindrical drop coordinates (r and z) and the radius of curvature at the drop apex (R_0). These parameters are crucial to analyze the interfacial tension out of the drop shape. Furthermore, the density of water and oil phase ($\Delta\rho$) and the gravity constant (g) are taken into account as drop shape influencing factors [28].

The Bond number and Worthington number are indicators for an accurate Young Laplace fitting and focus on the drop shape and the drop volume, respectively [28]. The Bond number is a part of the Young Laplace equation and estimates the drop shape for ideal Young Laplace fitting (eq. 2 [28]). If the Bond number is too small ($\ll 0.15$), the drop approaches a spherical shape, and the Young Laplace fitting is inaccurate [28].

$$Bo = \frac{\Delta\rho g R_0^2}{\gamma} \quad (2)$$

$$Wo = \frac{V_d}{V_{max}} \quad (3)$$

with

$$V_{max} = \frac{\pi D_n \gamma}{\Delta\rho g} \quad (4)$$

The Worthington number depends on the maximal drop volume (V_{max}) and the used drop volume (V_d) (eq. 3, [28]). V_{max} was defined by Harkins & Brown (1919) [36] and depends on the needle diameter ($D_n = 2$ mm), the interfacial tension (γ), the density difference ($\Delta\rho$) and the gravimetric constant (g) (eq. 4). This number can be used to find an appropriate drop volume to a given needle diameter for accurate Young Laplace fitting and should be very close to 1 [28].

Within short time adsorption behavior, a two fluid-needle was used to investigate the transport time of β -LG from the injection point to the oil/water interface (lag time) and the interfacial pressure after a certain time. A drop with water or with a solution of starch conversion products with 42 ± 0.1 μ L was formed and 3 ± 0.1 μ L of a solution of β -LG was injected to reach a protein concentration of 0.1% within the drop. The experiments were performed in triplicate. On the basis of Böttcher, Keppler, and Drusch (2017) and Schestkova et al. (2019) lag time was determined from the injection time point to the start point of decreasing interfacial tension [11, 37]. The analysis is influenced by injection induced motion with a low velocity field in the bulk phase. The lag time is not only diffusion based.

Long term adsorption behavior was measured by drop tensiometry (PAT1M, Sinterface Technologies e.K., Berlin, Germany) with a single needle at 22 °C. The interfacial tension was recorded for 14 h. The experiments were performed in triplicate.

Dilatational Rheology

Dilatational rheology was investigated by pendant drop tensiometry (PAT1M, Sinterface Technologies e.K., Berlin, Germany) at 22 °C. A high speed camera is used to record the drop shape during sinusoidal oscillation. All previously discussed key indicators (2–4) are still relevant.

Furthermore, the interfacial tension and the drop area are recorded and used to calculate the complex dilatational modulus [20] with Fourier analysis (eq. 5). This equation calculates the proportion of the change in interfacial tension (σ) and area (A).

$$E^* = \frac{d\sigma}{d\ln A} \quad (5)$$

An indicator of accuracy of the Fourier analysis is the harmonic distortion. The excitation-response behavior of the drop needs to be in linearity for a harmonic behavior. If the relationship is non-linear, the system shows non-harmonic distortion which can result in severe a calculation mistake [30]. The harmonic distortion was observed. All data represent a well-developed sinusoidal shape without non-harmonic distortion.

The accuracy of the dilatational measurement can be furthermore estimated with the capillary number (Ca , eq. 6). This number is an indicator for the frequency or amplitude limits [29] and depends on the bulk Newtonian viscosity of the drop and the surrounding liquid ($\Delta\mu$), the oscillation frequency (ω), the amplitude of volume oscillation (ΔV), the interfacial tension of the system (γ) and the capillary radius (a) [29]. The capillary number has to be $\ll 1$ to avoid viscous forces which might deform the drop and cause an inaccuracy in dilatational result calculation [29]. Furthermore, it is stated that Ca should be ideally < 0.002 to avoid any inaccuracy [29, 38].

$$Ca = \frac{\Delta\mu\omega\Delta V}{\gamma a^2} \quad (6)$$

During the dilatational rheology, a protein or protein/ starch conversion product solution drop of 30 mm³ was formed in MCT-oil with a viscosity of 30 mPas. The drop was equilibrated for 14 h (see long term adsorption). Afterwards, a frequency sweep (2.8% amplitude, 0.001 to 0.1 Hz) followed by an amplitude sweep (0.01 Hz, 0.7% to 7% amplitude) were performed. The experiments were performed in triplicate. The dilatational modulus E^* is calculated by the change in interfacial tension and the simultaneous change in drop area during sinusoidal expansion and compression within the sweeps. The elastic modulus (E') and viscous modulus (E'') are determined out of E^* (see eq. 7) [20]. The phase angle (ϕ) between the sinusoidal curves of interfacial tension and drop area is calculated with $\tan(\phi) = E''/E'$. If both curves are in phase, the interfacial film reacts only elastic. If there is a phase shift of 90° between the curves, the interfacial film reacts only viscous. A value between 0° and 90° shows a viscoelastic behavior of the film.

$$E^* = E_d + i\omega\eta_d = E' + iE'' \quad (7)$$

Lissajous-plots give further details in the viscoelastic behavior of interfacial films. These figures are plotted with the change in interfacial tension ($\Delta IFT = \sigma - \sigma_0$) versus the change

in area ($\Delta A/A_0$; $\Delta A = A - A_0$). σ_0 and A_0 represent the interfacial tension and area at zero strain.

Interfacial Shear Rheology

Interfacial shear rheology was performed with a Physica MCR301 and MCR102 rheometer (Anton Paar Germany GmbH, Ostfildern, Germany) provided with an interfacial bicone (Bicone, Bi-C68–5, Anton Paar Germany GmbH, Ostfildern, Germany) at 20 °C. The software-based calculations are based on records of interfacial angular velocity distributions and on the complex viscosity surface fluid model. According to the model requirements, the water and oil phase need to be Newtonian and the density and viscosity of both phases as well as the cell and bicone geometric data are taken into account [31]. The Boussinesq number (eq. 8) is an indicator of the bulk phase undesirable movement. The interfacial viscosity (η), the oil viscosity (η_o) and the protein or protein/starch conversion product solution viscosity ($\eta_{p/c}$) as well as the measurement cell radius (R) are considered for the calculations of the Boussinesq number [32]. If the Boussinesq number is higher than 1, the bicone induced movement is situated at the interface and not in the surrounding water and oil bulk phase [10]. However, the software automatically corrects the subphase drag for high and low Boussinesq numbers. Thus, this number will not be discussed in detail. More details about operating windows for oscillatory interfacial shear rheology can be found in other publications [39, 40].

$$Bou = \frac{\eta}{(\eta_o + \eta_{p/c})R} \quad (8)$$

During interfacial shear rheological measurements, the protein or protein/starch conversion product solution was carefully poured into the interfacial shear glass cylinder with the help of a glass rod. Bubbles were gently and immediately removed with pasteur pipettes. The bicone was positioned directly at the interface and covered with purified MCT-oil. The interfacial film development was monitored for 23 h at 1 Hz and 0.1% amplitude. Afterwards the film was investigated via frequency sweep (0.1% amplitude; 1–0.001 Hz) followed by amplitude sweep (0.3 Hz; 0.01% - 100% amplitude). The experiments were performed in triplicate. For comparison of the amplitude sweeps, the intersection points of $G' = G''$ were calculated with RHEOPLUS/32 Multi6 V3.62 (Anton Paar GmbH, Ostfildern, Germany). The complex shear modulus (G^*), the elastic modulus (G') and the viscous modulus (G'') are defined in a similar way as the dilatational moduli.

Statistical Analysis

Statistical analysis was performed by univariate ANOVA with significance measured by post-hoc Scheffé test ($p < 0.05$).

Results and Discussion

Molecular Composition of Starch Conversion Products

Figure 1 displays the chromatograms of the starch conversion products determined by means of SEC-MALS-DRI. The chromatograms of MD 14 and MD 9 are similar in terms of shape. Two main fractions can be distinguished between about 18 and 23 mL elution volume and about 23 and 26 mL reflecting different molecular size fractions. However, the relative portions differ strongly depending on the degree of molecular degradation. Increasing DE of the maltodextrin shifted the chromatogram to higher elution volume, indicating higher degree of degradation. Moreover, the ratio of the fractions changed remarkably. The chromatogram of GS 37 was distinct from the respective maltodextrin samples in terms of shape and position (elution volume range). In particular the chromatogram area between 24 and 26.5 mL relates to the maltose-rich (24–26 mL) and glucose-rich fractions (25–26.5 mL) [41]. Compared to the maltodextrins, the glucose syrup has a considerably higher mono- and disaccharide content as expected.

Physical Values of Solutions

Density and viscosity are recorded for all solutions (Table 1). The viscosity of the solutions increases with decreasing DE while the solutions show Newtonian behavior. This increase was differently pronounced in samples used for short time adsorption and interfacial rheology experiments owing to their different total starch conversion product concentrations. As expected, lower concentrations led to lower viscosities but also to a less pronounced increase in viscosity with decreasing

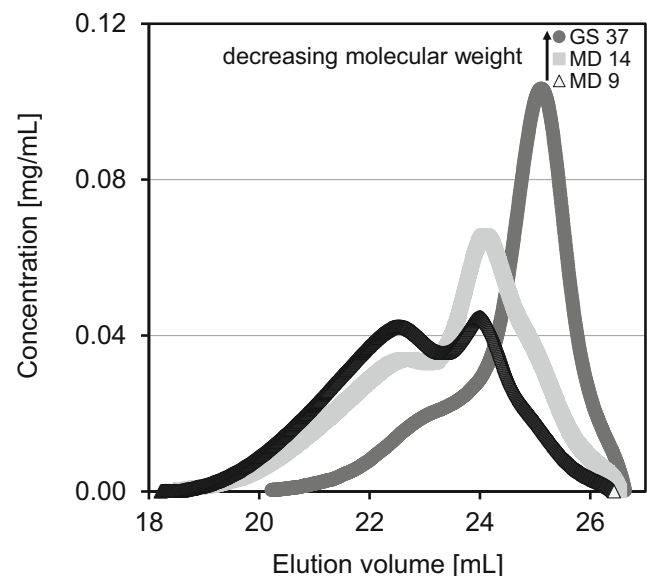


Fig. 1 SEC chromatogram of maltodextrin DE 9 (MD 9), 14 (MD14) and glucose syrup DE 37 (GS37)

DE (1.1 ± 0.0 mPas for β -LG to 5.4 ± 0.0 mPas for MD 9). In contrast at 35% concentration of protein and starch conversion products the viscosities ranged from 1.1 ± 0.1 mPas (β -LG) to 78.6 ± 2.5 mPas (MD 9). In earlier studies, it was shown that the viscosity is increasing in an exponential way especially for low DE with increasing concentration [18].

The density of a pure 0.1% or 1.5% β -LG solution was 1 g/cm³: With addition of 34.9% starch conversion products, the density increased to 1.15 or 1.16 g/cm³. All starch conversion product solutions with 15.95% showed a density of 1.06 g/cm³ (Table 1).

Calculation and Interpretation of Key Indicators for the Evaluation of Method Suitability

Precision of the determination of interfacial tension can be estimated with the Bond and Worthington number [28]. The Bond number (eq. 2) was calculated for the protein/starch conversion product solutions with a density difference of 0.21 g/cm³, an interfacial tension of 12 mN/m and a radius of approx. 1.93 mm which yields in a number of 0.64. Thus, the value of the Bond number lies above the critical value of 0.15. The calculated value of the Worthington number is with 0.82 close to the critical value of 1 (eq. 3). Furthermore, with volume increase of maximal 5 mm³ during oscillation the Worthington number will not be beyond the critical value. Therefore, Bond and Worthington number indicate an accurate determination of the interfacial tension in presence of starch conversion products at high concentrations.

For the dilatational rheology, the harmonic distortion and the capillary number are indicators for accurate measurements. All data showed harmonic distortion. The frequency limit for liquid-liquid interfaces was earlier stated to be 0.1 Hz [38]. Moreover, Freer et al. (2005) suggested the critical capillary number at $Ca < 0.002$ to neglect viscous forces [29]. This criterion applied for all investigated samples, amplitudes, and frequencies except for presence of MD 9 at 0.1 Hz and 2.8% amplitude which reached its maximum at $Ca = 0.0035$. Therefore, the affiliated data can be described as robust except for MD 9 at 0.1 Hz and 2.8% amplitude. Another indicator for amplitude limits in the dilatational measurement is a partially disrupted compression. A high viscosity of the solution can

hinder the full transfer of the downward movement of the piston in the drop tensiometer to decrease the drop volume. In this study the compression was partially disrupted for viscosities from 35 mPas and amplitudes above 4.2%. Above amplitudes of 4.2%, during compression the target amplitude was not reached occasionally. However, in interfacial tension-volume/area-time-graphs provided by the software measurements as well as target values can be controlled, and incorrect measurements can be excluded. We recommend avoiding these problems by adjustment of the pendant drop tensiometer equipment, for instance the capillary diameter and the pump performance hence pump volume.

The interfacial shear rheology is not susceptible to changes in physical characteristics like bulk viscosity, flow behavior or density. All these physical values are considered within the software based calculations [31]. Therefore, evaluation of interfacial properties of β -LG with presence of high dry matter content of 35% in the water phase is feasible with some limitations. Limitations might occur within the dilatational rheology for high amplitudes above 4.2%, and high frequencies of 0.1 Hz for highly viscous solutions (80 mPas). In general, indicators for measurement issues are a non-harmonic distortion of the drop, a partially disrupted compression, and a high capillary number. These indicators need to be observed critically during and after the measurement. Especially for a high capillary number and a disrupted compression, the data do not represent the reaction of the interfacial film on the target stress and should be excluded.

Time Dependent Adsorption Behavior

The first stage of the interfacial stabilization—migration of the protein to the interface—may be characterized via lag time and interfacial pressure after a defined time. Short time adsorption experiments have been performed with a two-fluid needle. The influence of starch conversion products with different DE on β -LG adsorption behavior is shown in Fig. 2. A significant increase in lag time with reduced DE reflecting an increased viscosity becomes obvious (Fig. 2a). The increase in viscosity due to the lowering degree of degradation of the starch conversion products slows the translational motion of the protein to the interface. This motion is affected by

Table 1 Physical values of protein and protein/starch conversion product solutions

| Sample | Viscosity [mPas] | Density [g/cm ³] | Sample | Viscosity [mPas] | Density [g/cm ³] |
|------------------|------------------|------------------------------|-----------------------------------|------------------|------------------------------|
| 0.1% β -LG | 1.1 ± 0.1^d | 1.00 ± 0.00^b | 1.5% β-LG | 1.1 ± 0.0^d | 1.00 ± 0.00^b |
| + 34.9% MD 9 | 78.6 ± 2.5^a | 1.16 ± 0.00^a | 15.96% MD 9 | 5.4 ± 0.0^a | 1.06 ± 0.00^a |
| + 34.9%MD 14 | 35.5 ± 0.8^b | 1.16 ± 0.00^a | 15.96% MD 14 | 3.6 ± 0.0^b | 1.06 ± 0.00^a |
| + 34.9% GS 37 | 7.9 ± 0.1^c | 1.15 ± 0.00^a | 15.96% GS 37 | 2.1 ± 0.0^c | 1.06 ± 0.00^a |

letters a-c indicate significant differences for all columns ($p < 0.05$)

the injection induced motion of the fluid which is influenced by the bulk viscosity according to the Navier-Stokes equation. However, comparison of our determined β -LG migration time with other literature is difficult due to the multitude of methods and influencing factors. Schestkova et al. (2019) and Böttcher et al. (2017) estimated a transportation time of around 5 s for 0.1% β -LG to the o/w interface with the same equipment [11, 37]. This increase of 4 s can be explained with their lower protein injection volume and lower water drop volume which causes less bulk motion. In comparison, these experimental conditions result in a lower velocity field than in our case.

Subsequently, the short time protein adsorption at the interface as second stage takes place. 12 s after protein injection, the interfacial pressure is similar for all samples and only β -LG in water and β -LG in MD 9 show a significant difference (Fig. 2b). Within such a short time, the results might be influenced by the velocity field due to protein injection and the lower total starch conversion product concentration. Thermodynamic effects between protein and polysaccharides cannot be discussed on the basis of the results of short time adsorption.

In long term adsorption studies after 14 h of equilibrating, interfacial tension was lower in samples with higher starch conversion product concentration, reduced degradation level and increasing viscosity (Fig. 3). Differences between MD14 and MD9 were not significant. Baeza et al. (2004) and Baeza et al. (2005) ascribed the reduction of surface tension to thermodynamic incompatibility of β -LG and several neutral polysaccharides [15, 16]. The underlying mechanisms are more noticeable due to ongoing conformational reorganization of the protein and the development of intermolecular interactions during stage 3 and 4 of interfacial stabilization, which in turn lead to phase separation with time. Perez et al. (2010) showed the same effect of decreased interfacial tension of β -LG at

pH 7 with addition of xanthan [17]. An increased tendency of incompatibility was described for globulins and neutral polysaccharide mixtures at a pH above the isoelectric point (pI) and high concentrations for both substances [42]. This thermodynamic incompatibility accompanies the local protein enrichment at the interface [13].

When β -Lg is the only component within the water phase of the emulsion, it tends to form intermolecular β -sheets at the interface [43]. It is assumed that the interfacial film with protein enrichment is densely packed with intermolecular β -sheets connecting the β -Lg molecules. Furthermore, the protein concentration around the interface is higher due to the protein enrichment. We therefore propose that a reduced interfacial tension is a result of the excluded volume effect [14]. A correlation between reduced surface tension and the excluded volume effect was indicated by second virial coefficient [14]. In addition, the decrease in interfacial tension was even more pronounced with decreasing dextrose equivalent and consequently decreasing level of degradation (Fig. 3). This can be mainly explained by the increase in molecular size which enhances thermodynamic incompatibility for MD 14 and MD 9 [44]. With increasing level of degradation, the proportion of mono- and disaccharides increases for GS 37 (Fig. 1). The role of mono- and disaccharides as conformational stabilizers of proteins was reported to be a result of steric exclusion to proteins, cohesive forces of mono- and disaccharides, and intra-molecular protein interactions as driving forces of clustering [45]. It was shown for a globular protein (lysozyme) that its hydration increased with increasing sugar concentration [46]. It can be assumed that for the glucose syrup the higher proportion of mono- and disaccharides compared to maltodextrins would result in a slightly lower protein enrichment and reduced thermodynamic incompatibility [47].

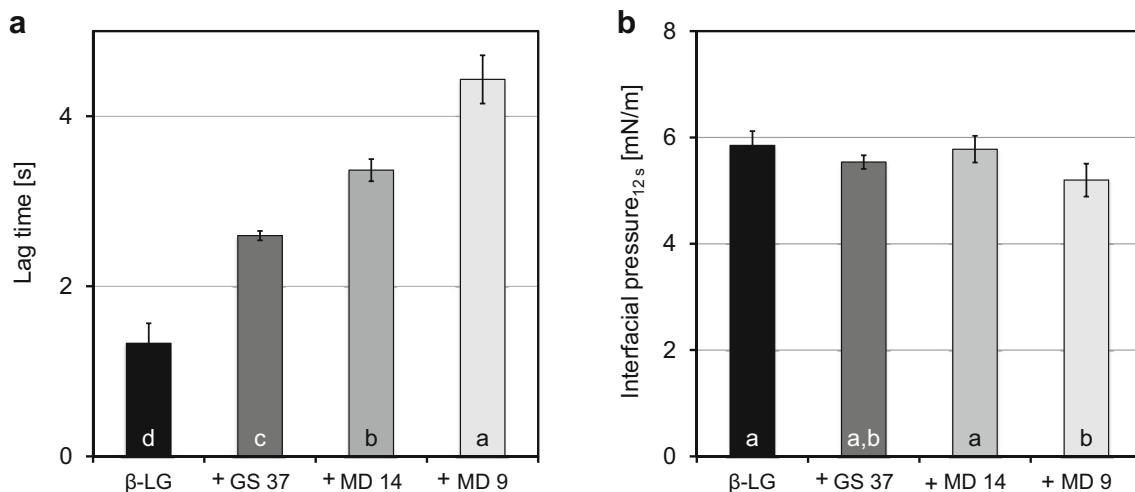


Fig. 2 a) Lag time and b) interfacial pressure 12 s after injection of 0.1% β -LG with presence of 14.9% glucose syrup (DE 37) and maltodextrin (DE 14 and 9) at MCT-oil/ water-interface, letters a-d indicate significant differences ($p < 0.05$)

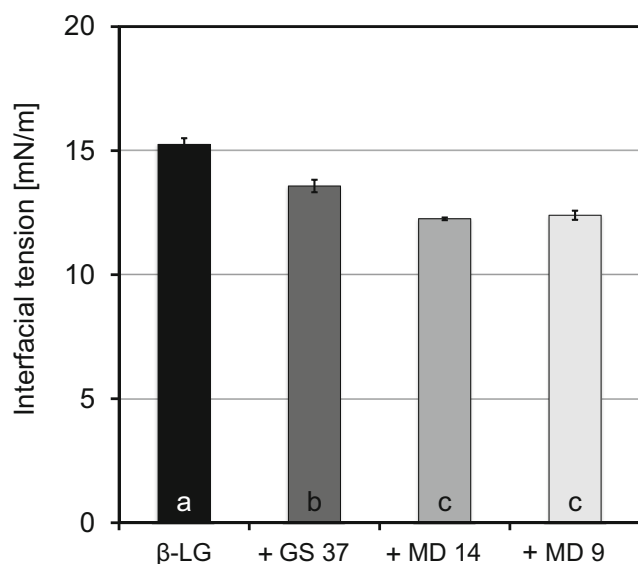
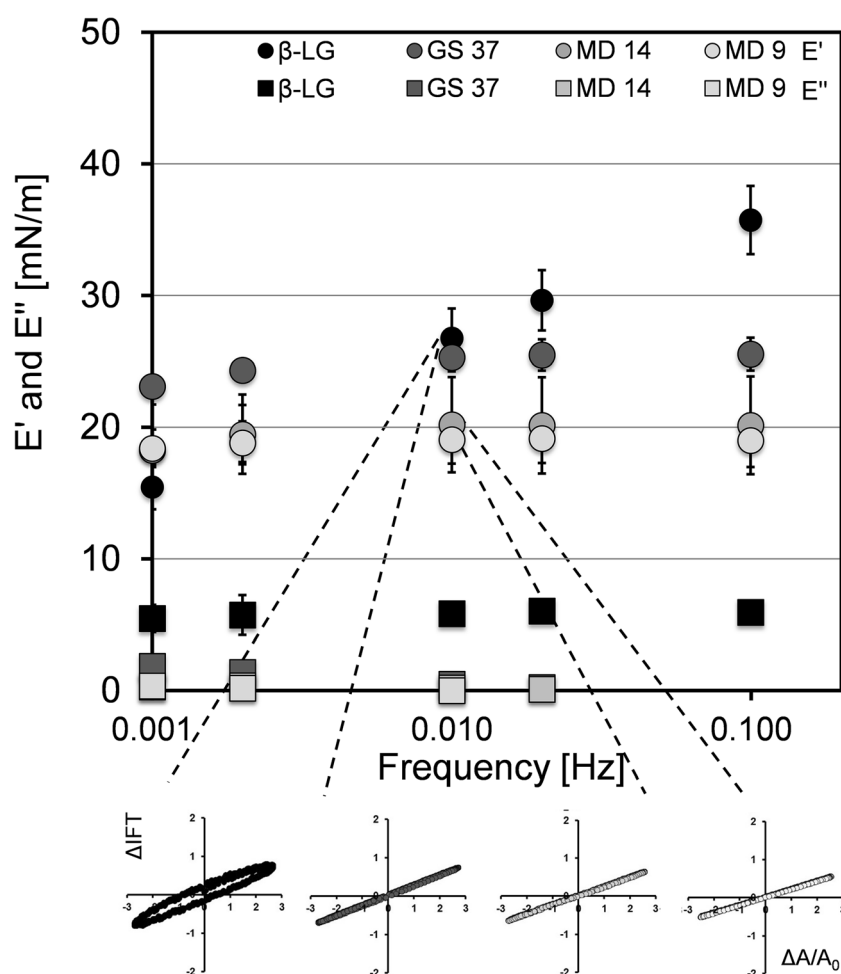


Fig. 3 Interfacial tension of 0.1% β-LG with presence of 34.9% glucose syrup (DE 37) and maltodextrin (DE 14 and DE 9) at MCT-oil/ water-interface after 14 h drop ripening, letters a-c indicate significant differences ($p < 0.05$)

Dilatational Rheology

The dilatational rheology is used to investigate the viscoelastic response of an equilibrated interfacial film to expansion and compression. The equilibrated film is characterized with a frequency sweep followed by an amplitude sweep. Within the frequency sweep, the β-LG-film shows an increase of the elastic modulus with higher frequencies (Fig. 4). With presence of starch conversion products, the elastic modulus remains nearly constant. At frequencies between 0.02 to 0.1 Hz, the elastic modulus is lower than for the pure β-LG. The viscous modulus decreases with presence of starch conversion products with no frequency dependence. Therefore, the typical viscoelastic behavior of β-LG is shifted to a more elastic response for all frequencies without difference in starch conversion products' DE (Lissajous-plots in Fig. 4). Furthermore, the phase angle for β-LG at 0.01 Hz is reduced with presence of starch conversion products with decreasing degradation level from $12.33^\circ \pm 1.62^\circ$, $1.08 \pm 0.73^\circ$, $0.52 \pm 0.47^\circ$ to $0.00 \pm 0.30^\circ$. With increasing frequency, only the phase angle of β-LG gradually increases from $9.46 \pm 0.90^\circ$ to $19.39 \pm 2.04^\circ$.

Fig. 4 Frequency sweep with elastic (E') and viscous (E'') moduli for 0.1% β-LG with presence of 34.9% glucose syrup (DE 37) and maltodextrin (DE 14 and DE 9) at MCT-oil/ water-interface, 2.8% amplitude 0.001–0.1 Hz after 14 h film formation and Lissajous-plots at 0.01 Hz



Within the amplitude sweep, β -LG shows a typical viscoelastic behavior with loss in elastic portions with increasing amplitude (Fig. 5). The presence of GS 37 shifts the viscoelastic behavior to a more elastic one (a_2 to c_2) with a phase angle of $0.39 \pm 0.71^\circ$ at 4.2% deformation. The presence of MD 14 and MD 9 results in a shift to a more elastic response (a_3 to c_3 and a_4 to c_4) with a phase angle of $-0.06 \pm 0.52^\circ$ and $0.05 \pm 0.26^\circ$ at 4.2% deformation, respectively. Nevertheless, MD 14 and MD 9 show partially a different behavior from amplitudes beyond 4.2%. In one case the compression of the β -LG/MD 14 drop is partially impeded from an amplitude of 5.6%. Changes within the length and orientation of the Lissajous-plot appeared in two cases from an amplitude of 6.3% (c_3). In the presence of MD 9 the compression is once incomplete from an amplitude of 4.9%. Once, the drop collapsed from an amplitude of 5.6%.

For all investigated frequencies and amplitudes, the more elastic response is shown in a linear Lissajous-plot and a phase angle around zero. The linear viscoelastic area ends at 6.3% amplitude with changes in orientation and length of the

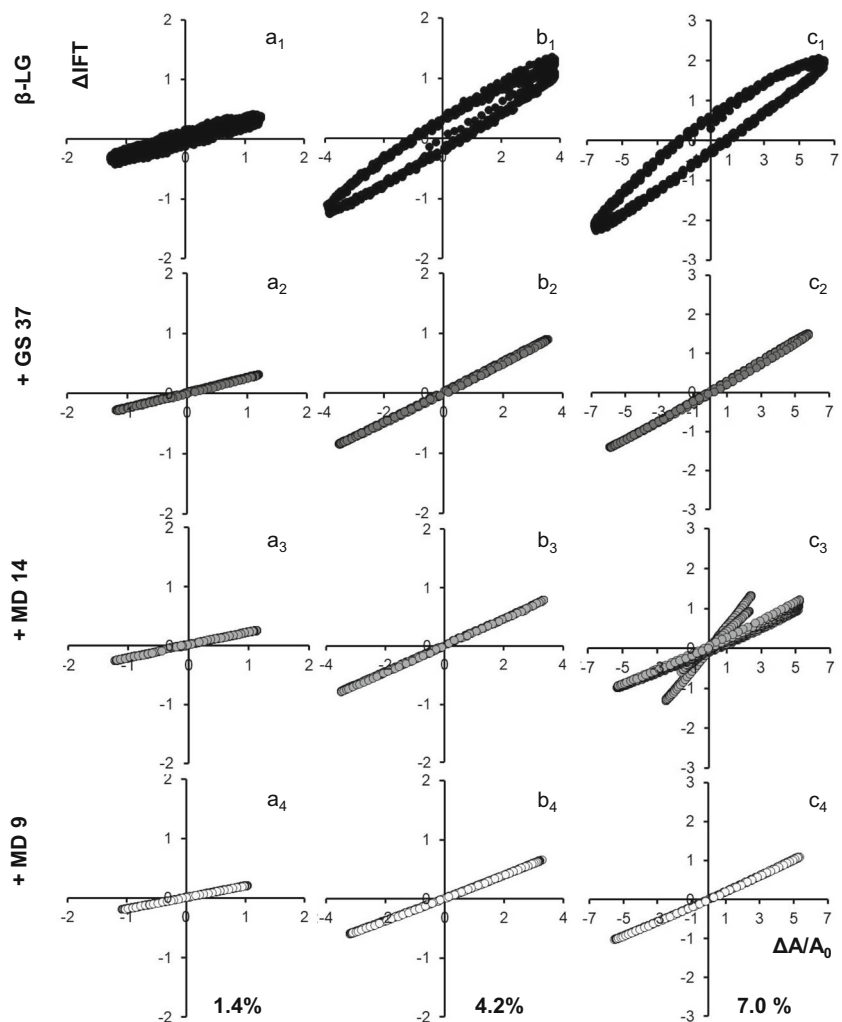
Lissajous-plots in the presence of MD 14. Baeza et al. (2004) and Perez et al. (2010) showed an increase in elastic response for β -LG with addition of xanthan as well but have not observed the end of the linear viscoelastic area [15, 17]. In comparison, the pure β -LG-film showed a frequency and amplitude dependent behavior in the dilatational rheology (Figs. 4 and 5), which was shown earlier [37, 48].

Interfacial Shear Rheology

The interfacial shear rheology is applied to analyze the viscoelastic interfacial network and its intermolecular interactions. One sample (β -LG and MD 9) showed a low G' . The sample might have been influenced by released water due to partial retrogradation [49].

The impact of starch conversion products' presence with varying DE onto the formation of β -LG-films is shown in Fig. 6a. At first, the interfacial film is formed and observed for 23 h. The elastic modulus with presence of GS 37 and MD 14 is significantly higher than the elastic modulus of β -LG

Fig. 5 Representative Lissajous-plots of amplitude sweep for 0.1% β -LG (a_1 to c_1) with presence of 34.9% glucose syrup (DE 37, (a_2 to c_2)) and maltodextrin (DE 14, (a_3 to c_3) and 9, (a_4 to c_4)) at MCT-oil/ water-interface, 1.4%, 4.2% and 7.0% amplitude and 0.01 Hz after 14 h film formation



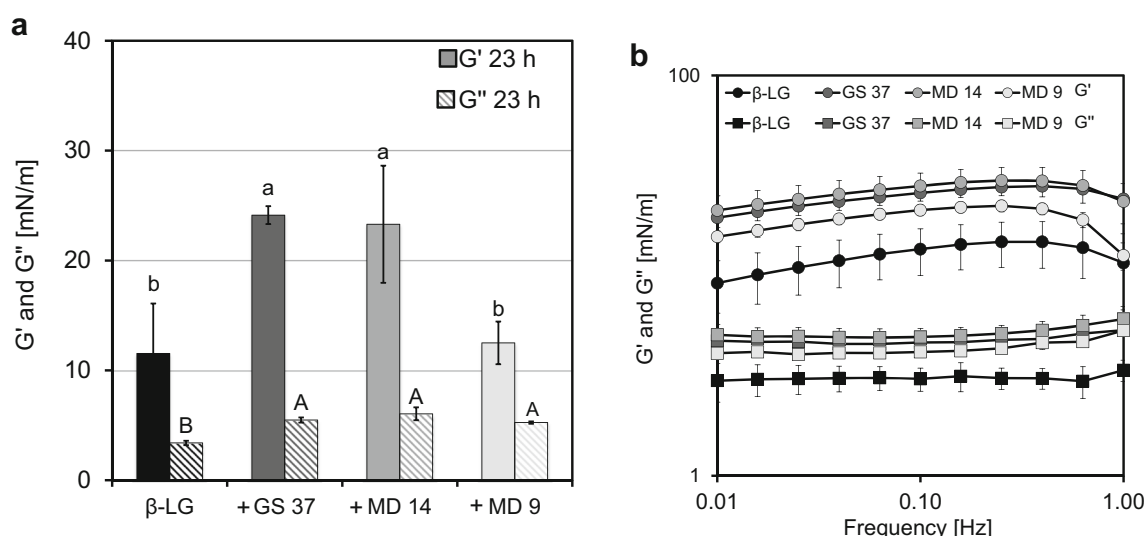


Fig. 6 a) Elastic (G') and viscous modulus (G'') of 23 h aged film and b) frequency sweep with elastic (G') and viscous (G'') moduli for 0.1% β -LG with presence of 34.9% glucose syrup (DE 37) and maltodextrin (DE

14 and 9) at MCT-oil/ water-interface, a) 1 Hz and 0.1% amplitude and b) 0.1% amplitude 0.01–1 Hz after 23 h film formation, letters a-b, A-B indicate significant differences ($p < 0.05$)

without presence of starch conversion products and with presence of MD 9 (Fig. 6a). The pairwise comparison reveals a significant difference for presence of all starch conversion products in comparison with β -LG in the viscous modulus. The formed interfacial films are further characterized via frequency (Fig. 6b) and amplitude sweep (Fig. 7).

Within the frequency sweep, differences in the curve progression of β -LG with and without presence of starch conversion products are shown (Fig. 6b). The elastic modulus is increasing linearly, and the viscous modulus remains constant from 0.01 to 0.25 Hz for all curves. From 0.25 Hz to 1 Hz, the viscous modulus starts to increase while the elastic modulus is reduced. This downturn of the elastic modulus can be

explained by instrument inertia which is explained in Ratdke et al. (2018) [50].

Within the amplitude sweep, differences in intersection point of G' and G'' are present (Fig. 7). Figure 7a shows the overall development of the elastic and viscous modulus while Fig. 7b pictures the intersection point of G' and G'' . Significant differences in the intersection point of G' and G'' for the y coordinate -G modulus- are shown with presence of MD 14 and GS 37 in comparison to β -LG (Fig. 7b). On trend, the G modulus is increased with presence of starch conversion products (Fig. 7b). While the x-coordinate in the intersection point -deformation- indicates no significant differences.

The elastic and viscous moduli increase significantly with presence of starch conversion products except for the

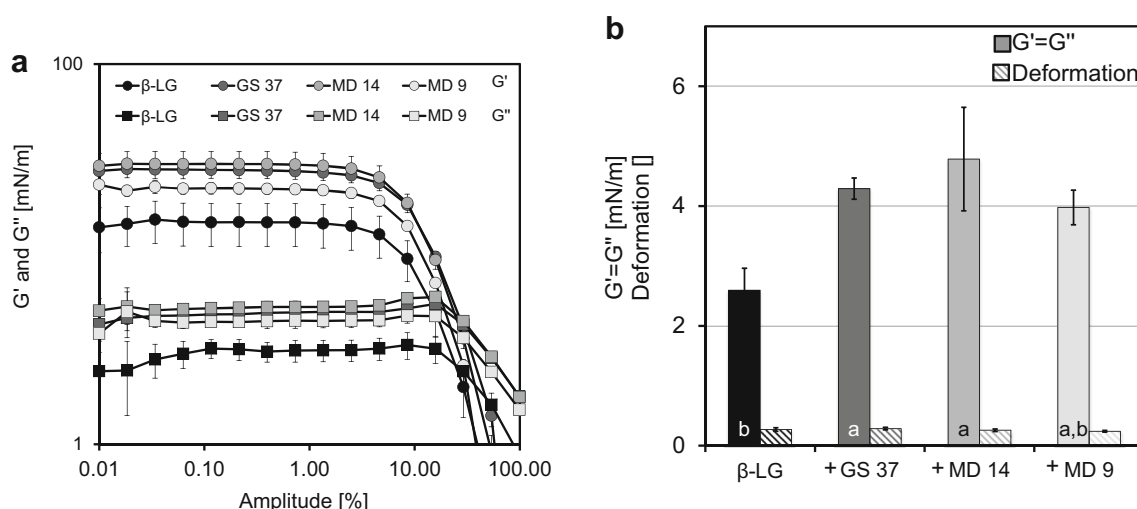


Fig. 7 a) Elastic (G') and viscous modulus (G'') of amplitude sweep with b) intersection point for 0.1% β -LG with presence of 34.9% glucose syrup (DE 37) and maltodextrin (DE 14 and 9) at MCT-oil/ water-interface 0.01–100% amplitude at 0.3 Hz, letters indicate significant differences ($p < 0.05$)

retrogradation influenced MD 9. Therefore, the different conformational reorganization and intermolecular interactions of stage 3 and 4 result in general in a strong network upon presence of starch conversion products.

Conclusion

This study focused on the impact of starch conversion products with varying dextrose equivalent at high concentrations on the interfacial properties of β -LG. It was shown that interfacial rheology can be applied at high dry matter content and that a complex interplay between formulation components of emulsions affect the interfacial characteristics. Moreover, interfacial rheology can be used to prove the impact of concentration depended effects like thermodynamic mechanisms.

In general, the presence of starch conversion products supports the formation of a stable interfacial film by the concentration depended excluded volume effect. Our suggestion, that the presence of starch conversion products would influence the interfacial properties of β -LG was confirmed by the increasing elasticity of the interfacial film with increasing intermolecular interactions. A low degree of degradation of starch conversion products resulted in extended protein enrichment at the interface, a high packing density in the film and a lower interfacial tension due to the increased thermodynamic incompatibility.

We assume that for a multicomponent system of oil, starch conversion products, milk proteins and low molecular weight emulsifiers like lecithins, citrem and mono- and diglycerides additional interactions between the oil phase and the low molecular weight emulsifier as well as interactions between the protein and the low molecular weight emulsifier will play a role in interfacial stabilization. Therefore, the impact of interactions between formulation components of spray dried emulsions on the interfacial properties of milk proteins needs to be investigated. The upcoming results will help to understand the mechanisms and interactions involved in the interfacial stabilization of spray dried emulsions which will have an impact on the stability of spray dried powders.

Acknowledgments The authors gratefully acknowledge the skillful lab-work of S. Gleisenberg (β -LG-isolation) and support of Dr. J. Keppler (analysis of β -LG quantification). Furthermore, M. Klost helped with her skillful proofreading of the manuscript. S. Heiden enriched the manuscript by illustrating the β -LG molecule.

Authors' Contributions • T. Heiden-Hecht: conceptualization, methodology, validation, formal analysis, investigation, writing-original draft, visualization, writing-review & editing.

• M. Brückner-Gühmann: supervision, validation, writing-original draft, writing-review & editing.

• S. Drusch: supervision, funding acquisition, writing-review & editing.

• M. Ulbrich: methodology, investigation – SEC-MALS-DRI.

Funding This IGF Project of the FEI was supported via AiF within the program for promoting the Industrial Collective Research (IGF) of the German Ministry of Economic Affairs and Energy (BMWi), based on a resolution of the German Parliament. We acknowledge the support by the German Research Foundation in this IGF Project (19312 N). Open Access funding enabled and organized by Projekt DEAL.

Compliance with Ethical Standards

Conflict of Interest The authors declare that they have no known competing financial interests or personal relationships that could have appeared to influence the work reported in this paper.

Open Access This article is licensed under a Creative Commons Attribution 4.0 International License, which permits use, sharing, adaptation, distribution and reproduction in any medium or format, as long as you give appropriate credit to the original author(s) and the source, provide a link to the Creative Commons licence, and indicate if changes were made. The images or other third party material in this article are included in the article's Creative Commons licence, unless indicated otherwise in a credit line to the material. If material is not included in the article's Creative Commons licence and your intended use is not permitted by statutory regulation or exceeds the permitted use, you will need to obtain permission directly from the copyright holder. To view a copy of this licence, visit <http://creativecommons.org/licenses/by/4.0/>.

References

1. R.S.H. Lam, M.T. Nickerson, *Food Chem.* **141**(2), 975–984 (2013)
2. E. Dickinson, *Food Hydrocoll.* **25**(8), 1966–1983 (2011)
3. G. Yampolskaya, D. Platikanov, *Adv. Colloid Interf. Sci.* **128–130**, 159 (2006)
4. B.S. Murray, E. Dickinson, *Food Sci. Technol. Int.* **2**, 131 (1996)
5. J.-M. Jung, D.Z. Gunes, R. Mezzenga, *Langmuir* **26**(19), 15366–15375 (2010)
6. D.A. Kim, M. Cornec, G. Narsimhan, *J. Colloid Interface Sci.* **285**(1), 100–109 (2005)
7. A. Moro, G.D. Báez, G.A. Ballerini, P.A. Busti, N.J. Delorenzi, *Food Res. Int.* **51**(1), 1–7 (2013)
8. S. Roth, B.S. Murray, E. Dickinson, *J. Agric. Food Chem.* **48**(5), 1491–1497 (2000)
9. K. Engelhardt, M. Lexis, G. Gochev, C. Konnerth, R. Miller, N. Willenbacher, W. Peukert, B. Braunschweig, *Langmuir* **29**(37), 11646–11655 (2013)
10. P.A. Rühs, N. Scheuble, E.J. Windhab, R. Mezzenga, P. Fischer, *Langmuir* **28**(34), 12536–12543 (2012)
11. H. Schestkova, T. Wollborn, A. Westphal, A.M. Wagemans, U. Fritsching, S. Drusch, *J. Colloid Interface Sci.* **536**, 300–309 (2019)
12. C.G. de Kruif, R. Tuinier, *Food Hydrocoll.* **15**(4–6), 555–563 (2001)
13. J.M. Rodríguez Patino, A.M.R. Pilosof, *Food Hydrocoll.* **25**(8), 1925–1937 (2011)
14. A.S. Antipova, M.G. Semenova, *Food Hydrocoll.* **11**(1), 71–77 (1997)
15. R. Baeza, C. Carrera Sanchez, A.M.R. Pilosof, J.M. Rodríguez Patino, *Food Hydrocoll.* **18**(6), 959–966 (2004)
16. R. Baeza, C. Carrera Sanchez, A.M.R. Pilosof, J.M. Rodríguez Patino, *Food Hydrocoll.* **19**(2), 239–248 (2005)
17. A.A. Perez, C. Carrera Sánchez, J.M. Rodríguez Patino, A.C. Rubiolo, L.G. Santiago, *Colloids Surfaces B Biointerfaces* **81**(1), 50–57 (2010)

18. P. Dokic, J. Jakovljevic, L. Dokic-Baucal, *Colloids Surfaces A Physicochem. Eng. Asp.* **141**(3), 435–440 (1998)
19. A.F.H. Ward, L. Tordai, *J. Chem. Phys.* **14**(7), 453–461 (1946)
20. E.H. Lucassen-Reynders, *Food Struct.* **12**, 1 (1993)
21. J. Krägel, S.R. Derkatch, R. Miller, *Adv. Colloid Interf. Sci.* **144**(1–2), 38–53 (2008)
22. F. Tamm, G. Sauer, M. Scampicchio, S. Drusch, *Food Hydrocoll.* **27**(2), 371–377 (2012)
23. R. Miller, J.K. Ferri, A. Javadi, J. Krägel, N. Mucic, R. Wüstneck, *Colloid Polym. Sci.* **288**(9), 937–950 (2010)
24. P. Bertsch, P. Fischer, *Langmuir* **36**(13), 3676 (2020)
25. P. Bertsch, P. Fischer, *Langmuir* **35**(24), 7937–7943 (2019)
26. P. Bertsch, M. Diener, J. Adamcik, N. Scheuble, T. Geue, R. Mezzenga, P. Fischer, *Langmuir* **34**(50), 15195–15202 (2018)
27. P. Bertsch, M. Diener, J. Adamcik, N. Scheuble, T. Geue, R. Mezzenga, P. Fischer, *Langmuir* **36**(7), 1848–1849 (2020)
28. J.D. Berry, M.J. Neeson, R.R. Dagastine, D.Y.C. Chan, R.F. Tabor, *J. Colloid Interface Sci.* **454**, 226–237 (2015)
29. E.M. Freer, H. Wong, C.J. Radke, *J. Colloid Interface Sci.* **282**(1), 128–132 (2005)
30. G. Loglio, P. Pandolfini, R. Miller, A. Makievski, J. Krägel, F. Ravera, *Phys. Chem. Chem. Phys.* **6**(7), 1375–1379 (2004)
31. H.O. Lee, T.S. Jiang, K.S. Avramidis, *J. Colloid Interface Sci.* **146**(1), 90–122 (1991)
32. P. Erni, P. Fischer, E.J. Windhab, V. Kusnezov, H. Stettin, J. Läger, *Rev. Sci. Instrum.* **74**(11), 4916–4924 (2003)
33. J.K. Keppler, F.D. Sönnichsen, P.-C. Lorenzen, K. Schwarz, *Biochim. Biophys. Acta* **1844**(6), 1083–1093 (2014)
34. P. H. Blanchard and F. R. Katz, *Starch Hydrolysates* (chapter 4) in *Food Polysaccharides and Their Applications*, Second Edition, Eds. A.M. Stephen, G.O. Phillips, P.A. Williams (CRC Press, 2006)
35. M. Ulbrich, J.M. Daler, E. Flöter, *Carbohydr. Polym.* **219**, 172–180 (2019)
36. W.D. Harkins, F.E. Brown, *J. Am. Chem. Soc.* **41**(4), 499–524 (1919)
37. S. Böttcher, J.K. Keppler, S. Drusch, *Colloids Surfaces A Physicochem. Eng. Asp.* **518**, 46–56 (2017)
38. F. Ravera, G. Loglio, V.I. Kovalchuk, *Curr. Opin. Colloid Interface Sci.* **15**(4), 217–228 (2010)
39. D. Renggli, A. Aliche, R.H. Ewoldt, J. Vermant, *J. Rheol.* **64**(1), 141–160 (2020)
40. J. Tajuelo, M.A. Rubio, *J. Rheol.* **62**(1), 295–311 (2018)
41. M. Ulbrich, T.A. Terstegen, E. Flöter, *Starch/Stärke* **71**, 1 (2019)
42. V.Y. Grinberg, V.B. Tolstoguzov, *Food Hydrocoll.* **11**(2), 145–158 (1997)
43. H. Schestkova, S. Drusch, A.M. Wagemans, *Food Chem.* **302**, 125349 (2020)
44. M. Semenova and E. Dickinson, *Biopolymers in Food Colloids: Thermodynamics and Molecular Interactions* (Koninklijke Brill NV, Leiden, The Netherlands, 2010)
45. D. Shukla, C.P. Schneider, B.L. Trout, *Adv. Drug Deliv. Rev.* **63**(13), 1074–1085 (2011)
46. A. Lerbret, P. Bordat, F. Affouard, A. Hédoux, Y. Guinet, M. Descamps, *J. Phys. Chem. B* **111**(31), 9410–9420 (2007)
47. A.S. Antipova, M.G. Semenova, *Carbohydr. Polym.* **28**(4), 359–365 (1995)
48. P.A. Rühls, C. Affolter, E.J. Windhab, P. Fischer, *J. Rheol.* **57**(3), 1003–1022 (2013)
49. S. Wang, C. Li, L. Copeland, Q. Niu, S. Wang, *Compr. Rev. Food Sci. Food Saf.* **14**(5), 568–585 (2015)
50. T. Radtke, L. Böni, P. Bohnacker, M. Maggi-beba, P. Fischer, S. Kriemler, C. Benden, H. Dressel, *BMC Pulm. Med.* **18**, 1 (2018)

Publisher's Note Springer Nature remains neutral with regard to jurisdictional claims in published maps and institutional affiliations.